Global simulation of tropospheric O3-NOx-hydrocarbon chemistry: 1. Model formulation

Citation

Published Version

Permanent link

Terms of Use

Share Your Story

Global simulation of tropospheric O_3-NO_x-hydrocarbon chemistry
1. Model formulation

Yuhang Wang,[1] Daniel J. Jacob, and Jennifer A. Logan

Department of Earth and Planetary Sciences and Division of Engineering and Applied Sciences, Harvard University, Cambridge, Massachusetts

Abstract. We describe a global three-dimensional model for tropospheric O_3-NO_x-hydrocarbon chemistry with synoptic-scale resolution. A suite of 15 chemical tracers, including O_3, NO_x, PAN, HNO_3, CO, H_2O_2, and various hydrocarbons, is simulated in the model. For computational expediency, chemical production and loss of tracers are parameterized as polynomial functions to fit the results of a detailed O_3-NO_x-hydrocarbon mechanism. The model includes state-of-the-art inventories of anthropogenic emissions and process-based formulations of natural emissions and deposition that are tied to the model meteorology. Improvements are made to existing schemes for computing biogenic emissions of isoprene and NO. Our best estimates of global emissions include among others 42 Tg N yr^{-1} for NO_x (21 Tg N yr^{-1} from fossil fuel combustion, 12 Tg N yr^{-1} from biomass burning, 6 Tg N yr^{-1} from soils, and 3 Tg N yr^{-1} from lightning), and 37 Tg C yr^{-1} for acetone (1 Tg C yr^{-1} from industry, 9 Tg C yr^{-1} from biomass burning, 15 Tg C yr^{-1} from vegetation, and 12 Tg C yr^{-1} from oxidation of propane and higher alkanes).

1. Introduction

Ozone in the troposphere is supplied by transport from the stratosphere, and is produced within the troposphere during the oxidation of hydrocarbons and CO catalyzed by NO_x (NO + NO_2) and HO_x (OH + peroxy radicals). It is removed by photolysis, chemical reactions, and deposition to the surface. Increasing anthropogenic emissions of NO_x, hydrocarbons, and CO over the past century have caused appreciable increases of tropospheric ozone over industrial continents and probably over the globe [*Crutzen and Zimmermann*, 1991; *Martinerie et al.*, 1995; *World Meteorological Organization* (*WMO*), 1995]. This increase has important implications for regional air quality, global atmospheric chemistry, and climate change [*Thompson et al.*, 1990; *WMO*, 1995].

Our understanding of the factors controlling tropospheric ozone is still limited. The difficulty is due in part to the complexity of the chemistry and in part to the wide range in the lifetimes for ozone and its precursors (hours to weeks). Global models of tropospheric ozone need to resolve the coupling between chemistry and transport on synoptic scales [*Stordal et al.*, 1995]. The first global three-dimensional simulation of tropospheric ozone was presented by *Levy et al.* [1985]; it included transport from the stratosphere and deposition at the surface but no chemistry in the troposphere. *Crutzen and Zimmermann* [1991] and *Roelofs and Lelieveld* [1995] reported global ozone simulations including NO_x-CO-CH_4 chemistry in the troposphere but not accounting for the more complicated

nonmethane hydrocarbon (NMHC) chemistry. *Müller and Brasseur* [1995] included NMHCs in a global ozone model using monthly mean winds.

Our model attempts to improve on earlier efforts by (1) incorporating a detailed but computationally expedient representation of tropospheric chemistry including NMHCs, (2) resolving synoptic-scale transport using meteorological data from a general circulation model (GCM), and (3) including process-based descriptions of emissions and deposition formulated to be consistent with the model meteorology. This paper describes the model. A detailed evaluation of model results with observations of ozone and its precursors is presented by *Wang et al.* [this issue(a)], and the factors controlling tropospheric ozone are investigated using this model [*Wang et al.*, this issue(b)].

2. Model Framework

The model utilizes meteorological data archived from a GCM developed at the Goddard Institute for Space Studies (GISS) [*Hansen et al.*, 1983]. It has a resolution of 4° latitude by 5° longitude, with seven vertical layers in a σ coordinate extending from the surface to 150 mbar. The seven layers are centered approximately at 960, 895, 790, 635, 470, 320, and 200 mbar. The GCM contains two additional vertical layers above 150 mbar, which we use only for the specification of upper boundary flux conditions as discussed in section 5. The GCM data archive includes 4-hour averages of winds, total cloud optical depths, precipitation at the surface, mixed layer heights, and column frequencies of wet and dry convection, and 5-day averages of temperature, humidity, and vertical distributions of cloud optical depth, precipitation, and convective mass fluxes. Cloud reflectivities at 800, 500, and 200 mbar are derived from the vertical distribution of cloud optical depth following *Spivakovsky et al.* [1990a]. A more detailed description of the meteorological variables can be found in the work

---

of *Prather et al.* [1987], *Jacob et al.* [1993], and *Chin et al.* [1996]. The model has been used previously to simulate chemical tracers of atmospheric transport [*Prather et al.*, 1987; *Jacob et al.*, 1987; *Jacob and Prather*, 1990; *Balkanski and Jacob*, 1990; *Balkanski et al.*, 1992, 1993; *Koch et al.*, 1996], tropospheric OH [*Spivakovsky et al.*, 1990a], sulfate [*Chin et al.*, 1996], and ozone over North America [*Jacob et al.*, 1993; *Chin et al.*, 1994; *Horowitz et al.*, 1998; *Liang et al.*, 1998].

For this study, we used observed climatology to apply some corrections to the GCM meteorological fields. Monthly scaling factors were applied to the specific humidity in each grid box to match monthly mean data for 1986-1989 from the European Center for Medium-Range Weather Forecasts (ECMWF) model with a resolution of 1.5° longitude x 1.5° latitude x 14 vertical layers [*Trenberth*, 1992]. Surface air temperature and precipitation over land were scaled similarly to match the monthly 0.5°x0.5° climatology by *Leemans and Cramer* [1992]. Since diel temperature variability is lacking in our GCM data archive, we assumed that surface air temperature over land varies as a sinusoidal function that peaks in midafternoon with a diel amplitude for clear sky of 2 K in the tropics and 5 K in the extratropics [cf. *Conway and Liston*, 1990], decreasing linearly with overhead cloud cover. The daytime mixing heights over the tropical continents in the GCM are too low [*Chin et al.*, 1996], and we extend them to 2.5 km in daytime [*Browell et al.*, 1988; *Jacob and Wofsy*, 1988].

We transport 15 chemical tracers in the model to describe O_3-NO_x-CO-hydrocarbon chemistry (Table 1). Transporting O_x and NO_x as chemical families reduces the need for tracking many rapidly interchanging gases [*Jacob et al.*, 1989]. *Jacob et al.* [1993] included N_2O_5 and HNO_4 as part of the NO_x family in their simulation of summertime ozone over North America; separate transport of N_2O_5 and HNO_4 is necessary here owing to their long lifetimes at low temperatures in winter and in the upper troposphere. Alkanes ($\geq C_4$) and alkenes ($\geq C_3$) are grouped as two lumped families ALK4 and ALKE, taking

advantage of the similar O_x and HO_x yields of different NMHCs on a per carbon basis [*Jacob et al.*, 1989]. The chemistry of the ALK4 tracer is assumed to be that of a butane-pentane mixture [*Lurmann et al.*, 1986], while the chemistry of the ALKE tracer is assumed to be that of propene. Isoprene emitted by vegetation is transported separately from the other alkenes.

Ethane is treated as a separate tracer because of its importance for peroxyacetylnitrate (PAN) formation in the remote atmosphere [*Kanakidou et al.*, 1991]. Propane emission is included in the model as an equivalent source of acetone with a yield of 80% [*Singh et al.*, 1994]. Acetone and higher ketones (lumped as KET) are included as two additional tracers because of their importance for PAN and HO_x production in the upper troposphere [*Singh et al.*, 1995]. The chemistry of KET is assumed to be that of methylethyl ketone. A constant methane concentration is specified at 1.7 parts per million by volume (ppmv) throughout the model domain. Aldehydes and other short-lived species not included in Table 1 are assumed to be in chemical steady state during the day and either in steady state or inert (depending on the species) at night. Ethylene, terpenes, and aromatic compounds are neglected; sensitivity simulations indicate that they play little role in global or regional atmospheric chemistry.

The model solves the three-dimensional continuity equation for 15 tracers (Table 1) using operator splitting between transport and chemistry over 4-hour time steps. The chemical operator applied to tracer i ($i = 1, ..., n$; $n = 15$) includes contributions from chemical reactions, emissions, and dry deposition:

$$\frac{\partial m_i}{\partial t} = E_i + P_i \{m_j\} - (k_{d,i} + k_{c,i}\{m_j\}) \, m_i \qquad (1)$$

where m_i is the concentration of species i, E_i is the emission rate, P_i is the chemical production rate, and $k_{d,i}$ and $k_{c,i}$ are the first-order loss rate constants for dry deposition and chemical loss, respectively. Values for P_i and $k_{c,i}$ are obtained by solution to the chemical mechanism described in section 3, and are fitted for rapid computation to polynomial functions of the tracer concentrations $\{m_j\}$ ($j = 1, ..., n$) and of meteorological variables (see the appendix). The system of n coupled differential equations (1) is integrated over the 4-hour time step using a Runge-Kutta fourth-order method with 4-hour average values of E_i, $k_{d,i}$, and photolysis rate constants. The linear projection of equation (1) used in the standard Runge-Kutta method renders the scheme unstable for tracers with lifetimes shorter than the integration time step. In our model the projection is computed instead using the analytical (exponential decay) solution to equation (1), which ensures the stability and improves the accuracy of the integration [*Elliott et al.*, 1993]. Another difficulty arises in computing chemistry in the lower troposphere because PANs, N_2O_5, and HNO_4 may interchange rapidly with NO_x; when the lifetimes of these species are shorter than 2 hours, we group them with NO_x, solve equation (1) for the family, and repartition the family after integration on the basis of chemical steady state.

The removal of soluble tracers HNO_3 and H_2O_2 by wet deposition is calculated separately from the chemical operator following the scheme of *Balkanski et al.* [1993]. This scheme includes scavenging in convective updrafts and rainout and washout by nonconvective large-scale precipitation.

Table 1. Chemical Tracers in the Model

Tracer	Composition
O_x	$O_3 + O + NO_2 + HNO_4 + 2 \times NO_3 + 3 \times N_2O_5 + PANs$
NO_x	$NO + NO_2 + NO_3 + HNO_2$
N_2O_5	
HNO_4	
PANs	peroxyacylnitrates
Butylnitrate	lumped alkylnitrates[a]
HNO_3	
CO	
Ethane	
ALK4	lumped $\geq C_4$ alkanes[a]
ALKE	lumped $\geq C_3$ alkenes[a]
Isoprene	
Acetone	
KET	lumped $\geq C_4$ ketones[a]
H_2O_2	

Propane is included in the model as an equivalent emission of acetone with a yield of 80% [*Singh et al.*, 1994]. Methane concentration is specified as 1.7 ppmv.

[a]Lumping of individual compounds is done on a per carbon basis.

3. Chemistry

The Harvard chemical mechanism used in the model is based on recent compilations including those of *DeMore et al.* [1994] for inorganic and methane chemistry, *Atkinson et al.* [1992] for NMHC chemistry, and *Paulson and Seinfeld* [1992] for the oxidation of isoprene. The termolecular rate constant for the OH + NO_2 reaction is from *Donahue et al.* [1997]. The quantum yields of O^1D from ozone photolysis at 312-320 nm are from *Michelsen et al.* [1994], leading to an O^1D production rate in the tropical troposphere 20-40% higher than the recommendation of *DeMore et al.* [1994]. Photolysis of acetone is computed with updated quantum yields and absorption cross sections from *McKeen et al.* [1997]. The UV radiation intensities are computed with a six-stream radiative transfer code for the Rayleigh scattering atmosphere including cloud reflection and aerosol absorption [*Logan et al.*, 1981]; the aerosol optical depth for absorption is 0.1 at 310 nm varying inversely with wavelength. Climatological ozone columns are specified as a function of latitude and month [*Spivakovsky et al.*, 1990a]. The Harvard chemical mechanism has been compared in two recent studies with other mechanisms used in atmospheric chemistry models [*Olson et al.*, 1996; *Friedl*, 1997].

Hydrolysis of N_2O_5 to HNO_3 on aerosol surfaces is computed in the model as the collision rate of N_2O_5 with sulfate aerosol particles [*Dentener and Crutzen*, 1993] assuming a reaction probability of 0.1 [*DeMore et al.*, 1994]. Global three-dimensional distributions of monthly averaged mass concentrations of sulfate aerosols are specified from the model simulation of *Chin et al.* [1996], which used the same GCM. The aerosol surface area is estimated from the sulfate mass concentrations by assuming that particles have a dry radius of 0.1 μm and are present in the atmosphere as aqueous $(NH_4)HSO_4$ solutions [*Dentener and Crutzen*, 1993]. The molar fraction of water in an aerosol depends on relative humidity following Raoult's law [*Seinfeld*, 1986]. Aerosols are assumed to remain in a metastable liquid state below the deliquescence point of $(NH_4)HSO_4$ [*Tang and Munkelwitz*, 1994]. Aqueous phase HO_x chemistry in clouds is not included in the model since its effects on O_x and NO_x appear to be insignificant [*Liang and Jacob*, 1997].

4. Emissions

The model includes emissions from fuel combustion and industrial activities (NO_x, CO, NMHCs), biomass burning (NO_x, CO, NMHCs), vegetation (NMHCs), soils (NO_x), and lightning (NO_x). Table 2 gives the global emission inventories for the different tracers, and Figure 1 shows the distributions of NO_x emissions from fossil fuel combustion, biomass burning, lightning, and soils.

4.1. Fuel Combustion and Industrial Activities

A global NO_x emission inventory (21 Tg N yr^{-1}) from fossil fuel combustion has been compiled by the Global Emission Inventory Activity [*Benkovitz et al.*, 1996] with a 1°x1° resolution. We use the companion inventory compiled by M. T. Scholtz, K. A. Davidson, E. C. Voldner, and A. Li that gives inventories for four seasons (C. M. Benkovitz, personal communication, 1997) (Figure 1). We distribute these NO_x emissions evenly in the model mixed layer, with 10% as NO_2

Table 2. Emission Inventories in the Model

	Global	Northern Hemisphere	Southern Hemisphere
NO_x			
Fossil fuel combustion	21	20	1.2
Biomass burning	11.6	6.5	5.1
Soil	6.0	4.2	1.8
Lightning	3.0	1.7	1.3
Aircraft	0.51	0.47	0.04
Stratosphere[a]	0.10	0.06	0.04
Total	42	33	9.4
CO			
Fossil and wood fuel combustion, industry	520	480	40
Biomass burning	520	290	230
CH_4 oxidation[b]	800	460	340
NMHC oxidation[b]	290	170	120
Total	2130	1400	730
Ethane			
Industry	6.3	5.7	0.6
Biomass burning	2.5	1.4	1.1
Total	8.8	7.1	1.7
Propane[c]			
Industry	6.8	6.1	0.7
Biomass burning	1.0	0.92	0.08
Total	7.8	7.0	0.8
≥C_4 alkanes			
Industry	30	27	3
≥C_3 alkenes			
Industry	10.4	9	1.4
Biomass burning[d]	12.6	7	5.6
Total	23	16	7
Isoprene			
Vegetation	597	297	300
Acetone			
Industry	1.0	0.9	0.1
Biomass burning	8.9	5.0	3.9
Vegetation	15	7.5	7.5
Oxidation of propane	6.2	5.3	0.9
Oxidation of higher alkanes[b]	6.2	5.5	0.7
Total	37	24	13

Units are Tg N yr^{-1} for NO_x, Tg CO yr^{-1} for CO, and Tg C yr^{-1} for NMHCs.

[a]Downward transport of NO_x across the tropopause. This transport also supplies 0.38 Tg N yr^{-1} of HNO_3 globally.

[b]Computed within the model.

[c]Included in the model as a direct emission of acetone; the yield of acetone from oxidation of propane is specified as 80% [*Singh et al.*, 1994].

[d]Including 6 Tg C yr^{-1} of ≥C_2 aldehydes.

[*Environmental Protection Agency (EPA)*, 1989]. For NO emissions from subsonic aircraft, we adopted the 1992 monthly mean emission inventory compiled by *Baughcum et al.* [1996] and *Metwally* [1995]; the inventory has a resolution of 1°x1°x1 km, and the global source is 0.51 Tg N yr^{-1}.

Our global CO emission inventory includes 390 Tg CO yr^{-1} from fossil fuel combustion and industrial activities and 130 Tg CO yr^{-1} from wood fuel burning. The inventory has a resolution of 1°x1° and is aseasonal. Statistics for fossil fuel combustion and industrial processes were taken from an electronic database compiled by the United Nations (U.N.), which includes data for each fuel (e.g., coal, lignite, gasoline, diesel, residual fuel oil) in 32 consumption categories (e.g., power
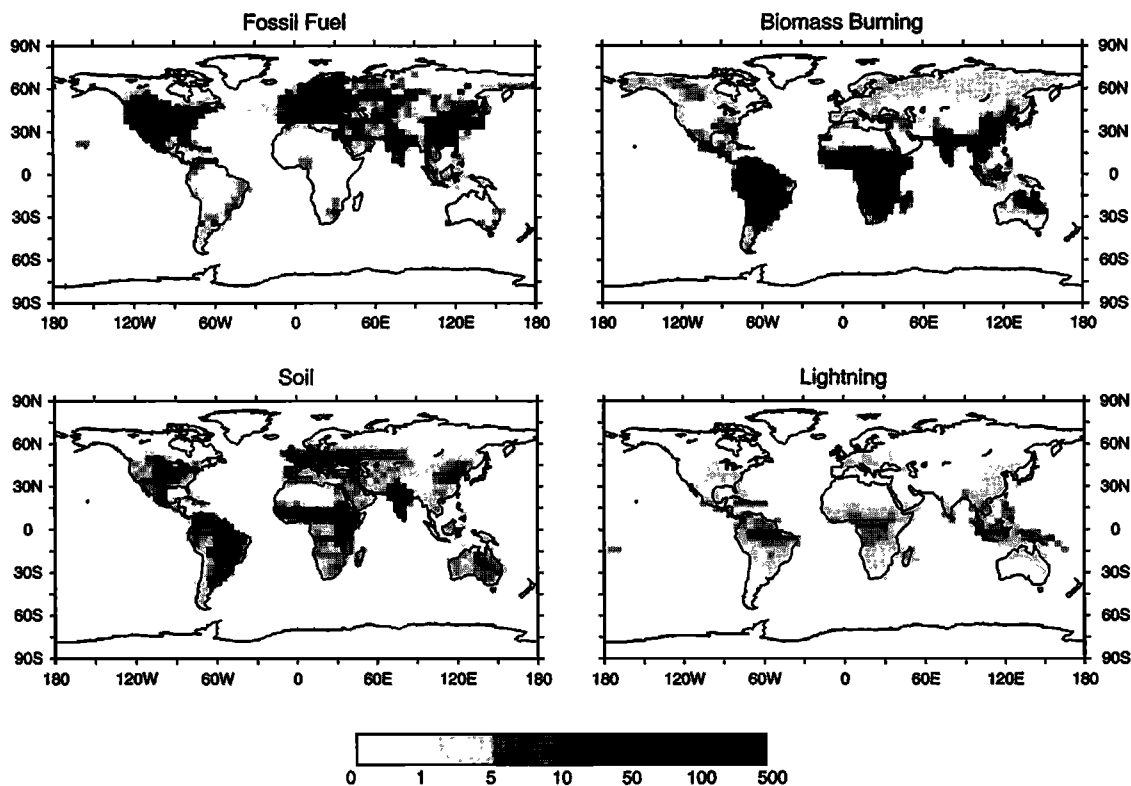
Figure 1. Annual mean emissions of NO_x (10^9 atoms N cm^{-2} s^{-1}) from fossil fuel combustion, biomass burning, soils, and lightning.

plants, road transportation, household). Data for countries not included in the U.N. database were supplemented with fuel statistics from the Organization for Economic Development and Cooperation if available; regional averages for fuel consumption patterns were used otherwise. Emission factors (the amount of CO produced per unit of fuel consumed) were taken from compendium AP-42 of the *Environmental Protection Agency* [1985, 1993] and from the European CORINAIR inventory [*Samaras and Zierock*, 1989]. Estimates for consumption of biomass fuels (wood, charcoal, dung, and agricultural residues) were based on published literature and on consultations with experts in energy consumption in developing countries. Emissions were derived by country and were spatially disaggregated using a 1° x 1° population map [*Benkovitz et al.*, 1996]. Exceptions are over the United States and Canada where recent estimates for national emissions of CO for 1985 [*EPA*, 1994] were scaled to the spatial distribution of CO emissions for 1985 from the National Acid Precipitation Assessment Program (NAPAP) [*EPA*, 1989]. Detailed descriptions of the inventory will be published separately.

We adopted the country-by-country inventory of *Piccot et al.* [1992] for emissions of paraffins (45 Tg C yr^{-1}) and olefins (18 Tg C yr^{-1}) from fossil fuel combustion and industrial activities. The emissions within each country were distributed on the basis of population density using a 1°x1° population map [*Benkovitz et al.*, 1996]. The *Piccot et al.* [1992] inventory gives no information on the speciation of paraffins and olefins; a speciation of emissions for the United States is, however, available from NAPAP [*Middleton et al.*, 1990]. The NAPAP data apportion total paraffin emissions over the United States on a per carbon basis as 6% ethane, 2% propane, 20% butanes,

68% ($\geq C_5$) alkanes, 2% acetone, and 2% higher ketones; olefin emissions are apportioned as 42% ethylene (not accounted for in the model) and 58% higher alkenes. There is evidence that the NAPAP inventory underestimates considerably the emissions of ethane and propane [*Rudolph*, 1995; *Goldan et al.*, 1995a]. Fresh pollution plumes sampled at Harvard Forest, Massachusetts, have typical ethane : propane : butanes (molar) concentration ratios of 1.4:1:1 in winter [*Goldstein et al.*, 1995], and winter urban air in Colorado has a propane to butanes molar ratio of about 1:1 [*Goldan et al.*, 1995a]. On the basis of the Harvard Forest data, we modify the NAPAP apportionment of paraffins on a per carbon basis to be 14% ethane, 15% propane, 66.5% ($\geq C_4$) alkanes, 2.3% acetone, and 2.2% higher ketones. Assuming the NMHC speciation for the United States to be globally representative, we deduce global emission rates of 6.3 Tg C yr^{-1} of ethane, 6.8 Tg C yr^{-1} of propane, 30 Tg C yr^{-1} of ($\geq C_4$) alkanes, 1.0 Tg C yr^{-1} of acetone, 1.0 Tg C yr^{-1} of higher ketones, and 10.4 Tg C yr^{-1} of ($\geq C_3$) alkenes.

4.2. Biomass Burning

Our global biomass burning emission inventory for CO has a 1°x1° spatial resolution and monthly temporal resolution. The global source totals 510 Tg CO yr^{-1}. The inventory incorporates estimates of forest wildfires (primarily at middle and high latitudes), tropical deforestation, slash/burn agriculture, savanna burning, and burning of agricultural waste. The methodology used is similar to that described by *Hao et al.* [1990] for tropical deforestation, *Logan et al.* [1981] for slash/burn agriculture, and *Menaut et al.* [1991] for savanna burning. Biomass burning, usually based on national information, was spa-

tially disaggregated within a country using the land use map of *Matthews* [1983]. The timing of biomass fires relies on wild-fire statistics at middle and high latitudes, on satellite monitoring of fires in Brazil (available electronically from INPE, Brazil) and Africa [e.g., *Cahoon et al.*, 1992], and on monthly rainfall data, with the fires occurring toward the end of the dry season if other information is lacking. A complete description of the biomass burning inventory will be in another publication currently in preparation by J. A. Logan.

Biomass burning emissions for other tracers are estimated by applying mean observed tracer emission ratios relative to CO. We use a global average NO$_x$ to CO molar emission ratio of 4.5% estimated by *Andreae et al.* [1996], which yields a global biomass burning source of 11.6 Tg N yr^{-1} (Figure 1). This source is comparable to the previous estimates of 12 Tg N yr^{-1} by *Logan* [1983] and 12.5 Tg N yr^{-1} by *Dignon and Penner* [1991] but 36% higher than the estimate of 8.5 Tg N yr^{-1} by *Levy et al.* [1991], who appear to have assumed a lower NO$_x$ to CO emission ratio.

Emission ratios of hydrocarbons to CO have been reported by a number of authors. We adopted average molar ratios of 0.55% for ethane to CO and 0.15% for propane to CO on the basis of measurements of fire plumes in North America [*Laursen et al.*, 1992; *Nance et al.*, 1993]. These ratios are in the range of values reported by *Lobert et al.* [1991] and *Hurst et al.* [1994]. The ethane to CO emission ratio is higher than the 0.4% measured by *Bonsang et al.* [1995] over the Ivory Coast. These references also indicate low emissions of ($\geq$ C$_4$) alkanes from fires. We adopted a ($\geq$C$_3$) alkenes to CO molar ratio of 0.79% based on a propene to CO molar ratio of 0.49% [*Lobert et al.*, 1991; *Laursen et al.*, 1992; *Nance et al.*, 1993; *Hurst et al.*, 1994] and a butene to CO emission ratio of 0.3% [*Lobert et al.*, 1991]. Molar emission ratios of 1.3% for acetone to CO, 3.1% for ($\geq$ C$_4$) ketones to CO, and 1.1% for C$_{2-3}$ aldehydes to CO were taken from *Mano* [1995] as cited by *Andreae et al.* [1996]. We choose to emit the C$_{2-3}$ aldehydes as ($\geq$C$_3$) alkenes on a per carbon basis since they have similar lifetimes and PAN yields [*Atkinson et al.*, 1992]. In summary, the hydrocarbon emissions from biomass burning in our model are 2.4 Tg C yr^{-1} of ethane, 1.0 Tg C yr^{-1} of propane, 8.9 Tg C yr^{-1} of acetone, 27 Tg C yr^{-1} of higher ketones, and 12 Tg yr^{-1} of ($\geq$C$_3$) alkenes. The large source of ketones is based on a single study and hence is subject to large uncertainty.

4.3. Vegetation

Large amounts of hydrocarbons are emitted from the terrestrial biosphere. Biogenic emissions from the oceans are estimated to be 2 orders of magnitude smaller [*Guenther et al.*, 1995]. Isoprene is the most important biogenic NMHC for O$_3$ production; terpenes are comparatively unimportant [*Fehsenfeld et al.*, 1992; *Cantrell et al.*, 1995]. We include in our model sources of isoprene and acetone from terrestrial vegetation.

We formulate isoprene emissions as a function of vegetation type, leaf area index (LAI, defined as square cm leaf area per square cm of surface), temperature, and solar radiation, using an algorithm developed by *Guenther et al.* [1995] with a few modifications described below. The global surface-type map is from *Oslon* [1992]; it has a spatial resolution of 0.5°x0.5° and distinguishes among 56 ecosystems. *Guenther et al.* [1995] assigned to each of the 56 ecosystems a base isoprene emission flux per unit leaf area (ϕ_o) at 30°C and for a

photosynthetically active radiation (PAR) flux of 1000 µmol m^{-2} s^{-1}. We adopted their ϕ_o values. The integrated isoprene emission flux Φ from a vegetation canopy is given by

$$\Phi = \phi_o \cdot LAI_{eff} \cdot f(T) \qquad (2)$$

$$LAI_{eff} = \int_0^{LAI} g(PAR)dL \qquad (3)$$

where $f(T)$ is a correction function for surface air temperature T, $g(PAR)$ is a correction function for the local photosynthetically active radiation (PAR) incident on the leaf, LAI is the leaf area index of the canopy, and LAI$_{eff}$ is the effective leaf area index corrected for light attenuation (and hence reduced isoprene emission) inside the canopy. The functions $f(T)$ and $g(PAR)$ are taken from *Guenther et al.* [1995].

The LAI values for each 0.5°x0.5° grid square of the *Olson* [1992] map are calculated monthly as a function of ecosystem type, net primary productivity (NPP), and global vegetation index (GVI). The NPP is calculated from monthly mean climatologies of surface temperature and precipitation. The computations of LAI and NPP follow the algorithms by *Guenther et al.* [1995] with two exceptions. First, we use monthly mean GVIs from the 0.5°x0.5°, 5-year *EDC-NESDIS* [1992] data set (*Guenther et al.* [1995] used the data for 1990 only). Second, we do not allow LAIs to exceed the mean growing season values for different ecosystems reported by *Lieth* [1975] and *Box* [1981]. The *Guenther et al.* [1995] algorithm calculates mean growing season LAIs that are much higher than those observed for certain ecosystems, for example, 11 and 6.3 for tropical rain forest and savanna, respectively; observed values reported by *Lieth* [1975] and *Box* [1981] for these ecosystems are 8 and 4, respectively. Our correction to LAIs has, however, only a small effect on the isoprene emission fluxes owing to attenuation of PAR inside the optically thick canopy.

We calculate the vertical profile of PAR inside the canopy using the canopy radiation transfer model of *Norman* [1982], as in the work of *Guenther et al.* [1995]. The total (direct and diffusive) PAR at a canopy top is calculated on the basis of the solar zenith angle θ and the opaque cloud fraction C. The can-
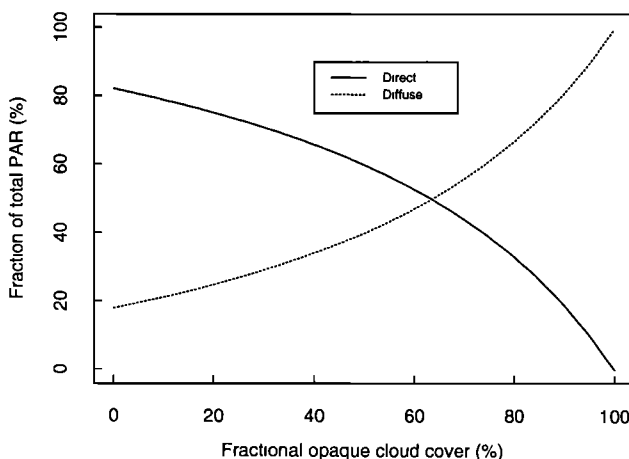

Figure 2. Partitioning of PAR between direct and diffuse components at the canopy top as a function of opaque cloud cover, computed using the radiative transfer model of *Norton* [1996] for a solar zenith angle of 30°.

opy radiative model of *Norman* [1982] calculates attenuation rates separately for direct and diffuse PAR and partitions leaf areas into shaded and sunlit fractions depending on overhead LAI and solar zenith angle; sunlit leaves receive both direct and diffuse PAR, while shaded leaves receive diffuse PAR only. *Guenther et al.* [1995] simplified the radiative transfer calculation by resolving the canopy into less than five vertical layers, and they employed an empirical formula to account for the effects of clouds on direct and diffuse PAR at the canopy top. In our work, we solve the radiative transfer equation inside the canopy more accurately, and we calculate diffuse and direct PAR at the canopy top as a function of solar zenith angle and overhead opaque cloud cover using a one-dimensional radiative transfer model for the atmosphere [*Norton*, 1996] (Figure 2). To speed up the computation in the three-dimensional model, we parameterized the effective leaf area index LAI_{eff} (equation (3)) as a polynomial function of LAI, θ, and C using the singular value decomposition method [*Press et al.*, 1992]. Figure 3 shows the dependence of LAI_{eff} on LAI for different solar zenith angles. The leveling-off of LAI_{eff} with increasing LAI reflects the attenuation of PAR inside the canopy and the accompanying decrease of isoprene emission by leaves.

The global distribution of isoprene emissions in our model (Figure 4) agrees qualitatively with *Guenther et al.* [1995], but our total isoprene emission of 597 Tg C yr⁻¹ is 20% higher. We attribute the difference largely to the inclusion of diel temperature variations in our model (section 2), which leads to higher daytime temperatures. Changes in temperatures on synoptic time scales in the GCM also contribute to higher isoprene emission in our model. Temperature variability increases isoprene emissions because of the near-exponential dependence of emissions on temperature up to 40°C.

Acetone also has a strong biogenic source, both from direct emissions and the oxidation of short-lived natural hydrocarbons [*Singh et al.*, 1994; *Goldan et al.*, 1995b]. *Singh et al.* [1994] estimated a global acetone source of 5 to 8 Tg C yr⁻¹ from direct biogenic emission and up to 6 Tg C yr⁻¹ from oxidation of biogenic hydrocarbons. We include in our model a total (direct and secondary) biogenic source for acetone of 15 Tg C yr⁻¹ adjusted to match observed acetone concentrations
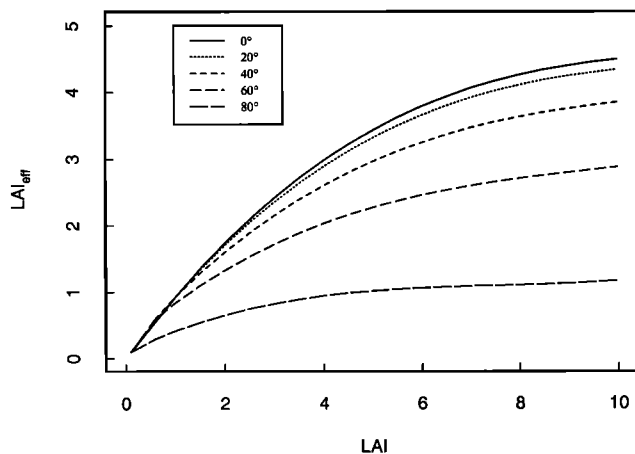

Figure 4. Monthly mean isoprene emission fluxes (10^{10} atoms C cm⁻² s⁻¹) computed in the model for January and July.

[*Wang et al.*, this issue(a)]. The temporal and spatial distribution of this acetone source is assumed identical to that of isoprene.

4.4. Soil NO_x Emissions

Nitrogen oxides are emitted by soil microbes during nitrification and denitrification processes. Following *Yienger and Levy* [1995], we compute NO emission fluxes as a function of vegetation type (from the *Olson* [1992] map), temperature, precipitation history, fertilizer usage if any, and a canopy reduction factor η. Parameter η is the fraction of soil-emitted NO_x that is deposited within the canopy before it is exported to the atmosphere; it reflects the oxidation of NO to NO_2 in the canopy air followed by uptake of NO_2 by vegetation [*Jacob and Bakwin*, 1991]. *Jacob and Bakwin* [1991] estimated η = 70% for the Amazon Forest based on concurrent measurements of soil emission fluxes and vertical profiles of NO and ozone concentrations inside the canopy. This result was extended by *Yienger and Levy* [1995] to other ecosystems by assuming an arbitrary function of LAI and stomatal area index (the product of LAI and the ratio of stomatal area to leaf area). We attempt here to formulate η on a more physical basis.

Following *Jacob and Bakwin* [1991], we express η as follows:

$$\eta = \frac{k_d}{k_v + k_d} \tag{4}$$

where k_d and k_v are the deposition and ventilation rate constants for NO_x in the canopy air, respectively; ventilation refers

Figure 3. Effective leaf area index LAI_{eff} for canopy emission of isoprene (equation (3)) as a function of LAI for different solar zenith angles and for clear sky.
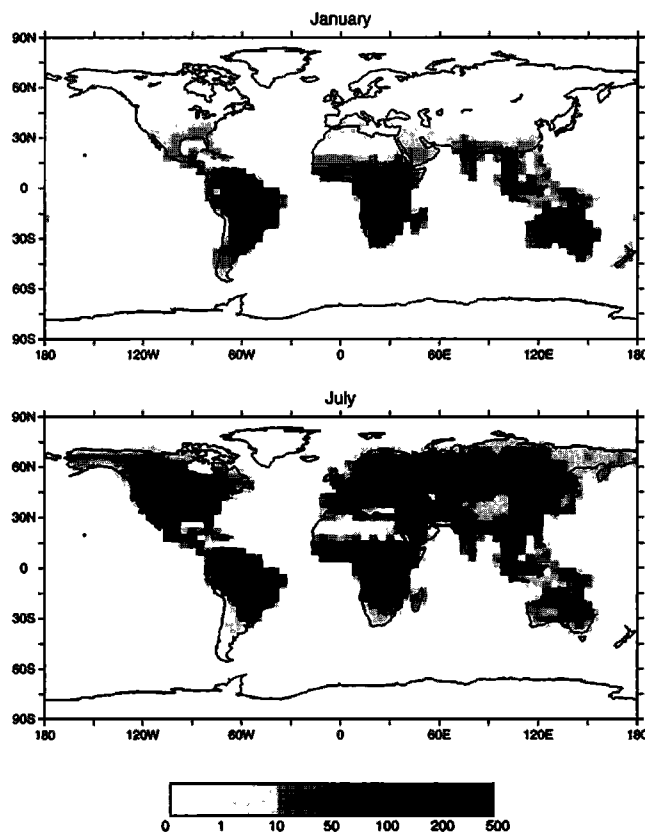
to the export of air from the canopy by turbulence. We compute k_d as

$$k_d = \frac{1}{R_c \cdot \Delta Z} \quad (5)$$

where R_c is the canopy surface resistance for deposition of NO_x and ΔZ is the canopy depth. Values of R_c are calculated in the model as part of the dry deposition algorithm described in section 6, assuming a NO_2 to NO_x concentration ratio of 0.7 inside the canopy [Jacob and Bakwin, 1991]. We compute the canopy ventilation rate constant k_v by assuming that it is proportional to the mean wind speed $\bar{v}$ inside the canopy:

$$k_v = \frac{\alpha \bar{v}}{\Delta Z} \quad (6)$$

where α is a dimensionless coefficient. Based on the micrometeorological model calculations reported by Shaw [1982], we parameterize $\bar{v}$ as:

$$\bar{v} = \min\left(\frac{V}{\gamma\sqrt{LAI}}, V\right) \quad (7)$$

where V is the above-canopy wind speed and γ is a nondimensional extinction coefficient which characterizes the rate at which wind speed decreases with depth in the canopy. Values of γ are 1, 2, and 4 for grass, shrub, and forest ecosystems, respectively [Shaw, 1982]. The coefficient α (2.8×10^{-2} and 5.6×10^{-3} for day and night, respectively) is adjusted to yield a canopy ventilation time of 1 hour during daytime and 5 hours at night for the Amazon Forest in April, as reported by Jacob and Bakwin [1991] (LAI = 7, ΔZ = 30 m, and V = 3 m s^{-1} [Fitzjarrald et al., 1990]).

We estimate in this manner a canopy reduction factor η = 70% for the Amazon Forest in April, as obtained by Jacob and Bakwin [1991]. However, our computed global average η is only 20%. Compared with the Amazon Forest, most ecosystems have smaller values of LAI and γ, stronger winds above the canopy, and higher canopy surface resistances for NO_2 deposition. Our global mean η is considerably less than the estimate of 50% by Yienger and Levy [1995]. Our global above-canopy emission of NO_x from soils is 6 Tg N yr^{-1} (Figure 1), only 10% higher than that of Yienger and Levy [1995], likely reflecting differences in the meteorological fields used for surface temperature and precipitation.

4.5. Lightning NO_x

Estimates of NO_x production from high-temperature fixation of N_2 by lightning are highly uncertain [Lawrence et al., 1995; Price et al., 1997a, b; Bradshaw et al., 1998]. Following the scheme of Price and Rind [1992], we compute frequencies of lightning flashes in our model based on the heights of local convective cloud tops from the GISS GCM. Price and Rind [1994] showed previously that the lightning frequencies derived in this manner from the GCM are in good agreement with satellite observations. We compute the intra-cloud (IC) to cloud-ground (CG) lightning flash ratio for a given grid square:

$$\frac{IC}{CG} = 2.7 \, F^{0.5} \quad (8)$$

where F is lightning frequency in flashes per minute [Rutledge et al., 1992]. The resulting global mean IC/CG flash ratio in our model is 7.7. The NO_x yield of a CG lightning flash is assumed to be 3 times that of an IC lightning flash because of higher flash energy [Liaw et al., 1990, and references therein]. We assume further that the amount of NO_x produced by a lightning flash is proportional to the channel length. We determine the CG lightning channel length in the model as the distance from the surface to the negative charge layer (NCL) where temperature is -10°C [Williams, 1985] and the IC channel length as the distance from the NCL to the convective cloud top. We thus obtain a global IC/CG NO_x emission ratio of 3.3. The vertical distribution of the lightning NO_x source is specified from cloud outflow simulations by K. E. Pickering (reported by Friedl [1997]) using a mesoscale cloud-ensemble model for tropical continental, tropical marine, and midlatitude continental convective systems. The resulting distribution is "C" shaped with 40-75% of lightning NO_x released in the top 3 km of convection and 1-20% released in the lowest 1 km above the surface depending on the type of convective system.

Our formulation of the lightning NO_x source, as described thus far, constrains the distribution of the source but not its magnitude. Penner et al. [1991] and Levy et al. [1996] have pointed out that measurements of NO, when interpreted with global three-dimensional model simulations, offer some constraints on the source strength. Following their approach, we adjusted the global source of NO from lightning in our model to match observations of NO from Drummond et al. [1988] and Smyth et al. [1996] in the upper troposphere over the northern equatorial Atlantic, where lightning influence on NO concentrations is particularly strong. Our resulting best estimate of the lightning NO_x source in the model is 3 Tg N yr^{-1} (Figure 1), the same as previously estimated by Levy et al. [1996] and Penner et al. [1991], who used different observations as constraints. There are, however, large uncertainties in these estimates as they are contingent on accurate model simulation of transport and chemistry of NO_x in the upper troposphere.

5. Transport of O_3 and Reactive Nitrogen From the Stratosphere

Flux upper boundary conditions are applied to the model at 150 mbar to represent the transport of O_3, NO_x, and HNO_3 from the stratosphere to the troposphere. At extratropical latitudes, the tropopause is lower than 150 mbar [Holton et al., 1995], and we take this difference into account in the analysis of model results in the companion papers.

The vertical resolution of the GISS GCM is too coarse for simulation of stratosphere-troposphere exchange [Spivakovsky and Balkanski, 1994]. We therefore constrain the cross-tropopause mass fluxes in our model using airflow climatology derived from observations [Holton et al., 1995; Appenzeller et al., 1996]. Appenzeller et al. [1996] showed that the cross-tropopause air mass flux has a May-June peak in the northern hemisphere but an austral winter peak in the southern hemisphere. We specify the relative seasonal variation of the cross-tropopause flux of ozone in each hemisphere as the product of the monthly cross-tropopause air mass fluxes given by Appenzeller et al. [1996] and the monthly climatological ozone concentrations at 100 mbar at midlatitudes (J. A. Logan, An analysis of ozonesonde data, 1, Its application in testing models of tropospheric chemistry, manuscript in preparation, 1998). We choose to retain the spatial distribution of the cross-tropopause ozone flux derived from the GISS GCM transport; 80-90% of the flux in each hemisphere is between 20° and 60°
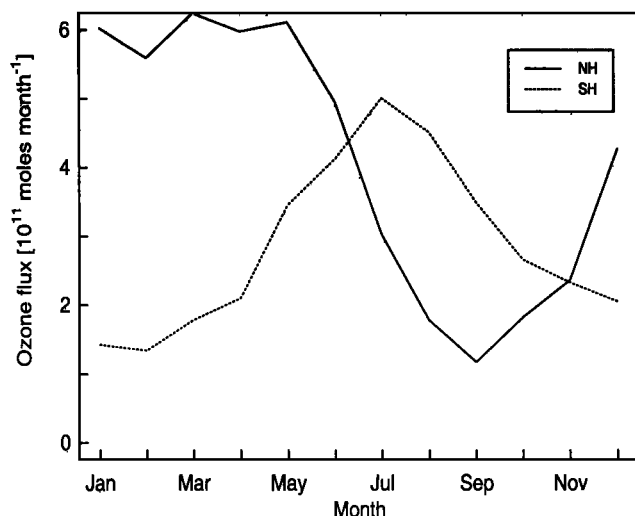
Figure 5. Monthly mean downward fluxes of ozone across the tropopause specified in the model for the northern (NH) and southern hemispheres (SH).

latitude, the remainder is at higher latitudes, and downward transport in the tropics is negligible, consistent with current knowledge [*Holton et al.*, 1995]. The relative seasonal and spatial distribution of the cross-tropopause ozone flux is then scaled to a global mean cross-tropopause flux in the model so as to match ozonesonde observations at middle and high latitudes in the winter northern hemisphere.

We obtain in this manner annual mean cross-tropopause ozone fluxes of 5×10^{12} mol yr^{-1} and 3.5×10^{12} mol yr^{-1} in the northern and southern hemispheres, respectively. Figure 5 shows the monthly mean fluxes in each hemisphere. Our values are at the lower end of those reviewed by *Fishman* [1985] and *Warneck* [1988], which range from 5×10^{12} to 11×10^{12} mol yr^{-1} in the northern hemisphere and from 3×10^{12} to 6×10^{12} mol yr^{-1} in the southern hemisphere. Our global flux of 8.5×10^{12} mol yr^{-1} is 20% lower than the value of 11×10^{12} mol yr^{-1} used in two recent tropospheric ozone models [*Müller and Brasseur*, 1995; *Roelofs and Lelieveld*, 1995].

Reactive nitrogen oxides produced from the oxidation of N_2O in the stratosphere are also transported across the tropopause. The cross-tropopause flux boundary condition for total reactive nitrogen (NO_y) is prescribed by scaling the estimated ozone fluxes with a NO_y/O_3 concentration ratio of 0.4% observed in the lowermost stratosphere [*Murphy et al.*, 1993]. A flux of 0.48 Tg N yr^{-1} of NO_y is computed, similar to the estimate made by *Ko et al.* [1991] from mass balance considerations for N_2O. The NO_y transported across the tropopause is assumed to consist of NO_x and HNO_3 with a molar ratio of 1:4 [*McElroy et al.*, 1992].

6. Dry Deposition

We use a resistance-in-series model [*Wesely and Hicks*, 1977] to compute dry deposition velocities of O_3, NO_2, HNO_3, PANs, and H_2O_2. The deposition velocity V_i for species i is computed as

$$V_i = \frac{1}{R_a + R_{b,i} + R_{c,i}} \qquad (9)$$

where R_a is the aerodynamic resistance to transfer to the surface, $R_{b,i}$ is the boundary resistance, and $R_{c,i}$ is the canopy sur-

face resistance. R_a and $R_{b,i}$ are calculated from the GCM meteorological variables [*Jacob et al.*, 1993]. Surface resistances $R_{c,i}$ for different species and for different surface types are based largely on the canopy model of *Wesely* [1989] with some improvements, including explicit dependence of canopy stomatal resistances on LAI [*Gao and Wesely*, 1995] and on direct and diffuse PAR within the canopy [*Baldocchi et al.*, 1987]. The same radiative transfer model for direct and diffuse PAR in the canopy is used as in the formulation of isoprene emissions (section 4). Surface resistances for deposition to tropical rain forest and tundra are taken from *Jacob and Wofsy* [1990] and *Jacob et al.* [1992], respectively. The surface resistance for deposition of NO_2 is taken to be the same as that of ozone [*Erisman and Pul*, 1994; *Kramm et al.*, 1995; *Eugster and Hesterberg*, 1996] and hence lower than specified by *Wesely* [1989]. Dry deposition of CO and hydrocarbons is negligibly small and not included in the model [*Müller and Brasseur*, 1995].

Figure 6 shows the simulated 24-hour average deposition velocities of ozone and HNO_3 in July. Deposition velocities of ozone are much lower over the oceans (<0.05 cm s^{-1}) than over the continents (0.1-1 cm s^{-1}) because of the poor solubility of ozone in water. Nitric acid has much higher deposition velocities (0.2-5 cm s^{-1}), reflecting a lack of surface resistance. The high ozone deposition velocities over the Amazon Forest (1-1.8 cm s^{-1} in daytime) are consistent with the observations of *Fan et al.* [1990]. We compared the seasonal variation of the ozone deposition velocity in the model to long-term observations by *Munger et al.* [1996] at Harvard Forest, Massachu-
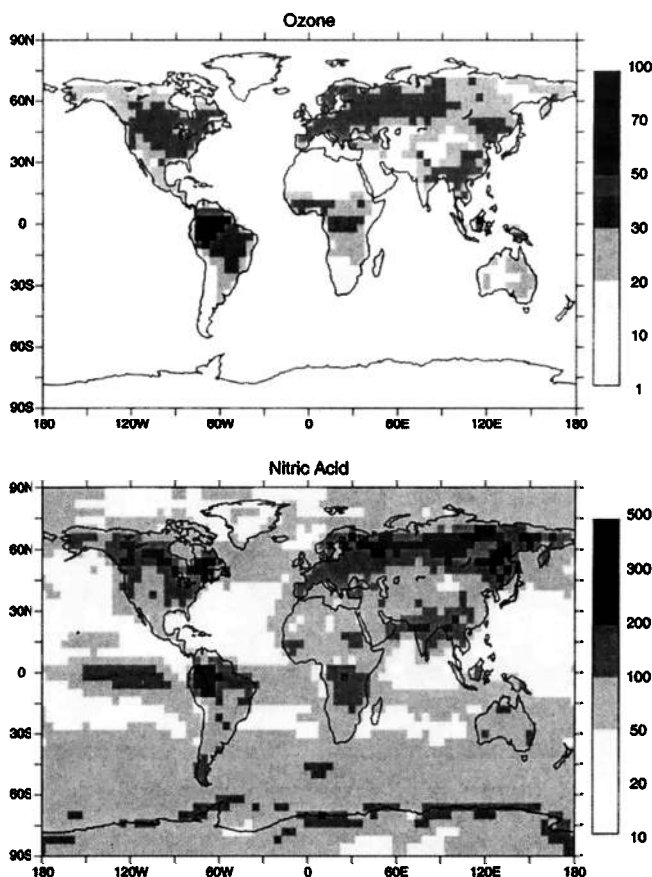

Figure 6. Twenty-four-hour average deposition velocities (10^{-2} cm s^{-1}) for ozone and HNO_3 at 250 m above the surface in July.

setts. The simulated ozone deposition velocities at that location peak in summer (0.4-0.8 cm s⁻¹ in daytime, <0.2 cm s⁻¹ at night) and decrease in winter to less than 0.2 cm s⁻¹ for both day and night, in good agreement with the observed values.

7. Conclusions

We have described the formulation of a global three-dimensional model for tropospheric chemistry. The model transports 15 chemical tracers and includes a detailed O_3-NO_x-hydrocarbon mechanism. Integration of this mechanism is made computationally expedient through the use of parameterized polynomial functions for production and loss rates of tracers. A 1-year simulation on a 72x46x7 grid takes 22 CPU hours on an IBM RS6000 workstation (model 39H) with a single processor; 50% of the CPU time is spent on the chemical integration.

The model includes state-of-the-art inventories of anthropogenic emissions from fuel combustion, industrial activities, and biomass burning. The formulations for natural emissions and deposition are process based and are tied to the underlying model meteorology and observed climatologies. Isoprene emission from vegetation is computed using the algorithm of *Guenther et al.* [1995] with improved representations of LAI and canopy radiation transfer; our global isoprene source (597 Tg C yr⁻¹) is 20% higher than that given by *Guenther et al.* [1995]. Emission of NO_x from soils is computed using the scheme of *Yienger and Levy* [1995]; we improve their simple parameterization of the canopy reduction factor with a more physical model based on the work of *Jacob and Bakwin* [1991]. We obtain a global mean canopy reduction factor of 20%. Our global above-canopy NO_x source of 6 Tg N yr⁻¹ is 10% higher than that given by *Yienger and Levy* [1995]. We estimate a global source of 3 Tg N yr⁻¹ of NO_x by lightning, in good agreement with *Levy et al.* [1996] and *Penner et al.* [1991] and at the lower end of the 2-10 Tg N yr⁻¹ range reviewed by *Bradshaw et al.* [1998].

We took a simple approach in estimating the NO_x emissions from biomass burning by applying an average NO_x to CO emission ratio [*Andreae et al.*, 1996] to the CO emission inventory. The resulting NO_x source is 11.6 Tg N yr⁻¹, at the high end of 7-13 Tg N yr⁻¹ reported by the *WMO* [1995]. A better approach would be to use the observed correlation of NO_x to CO_2 emission ratios with the N/C ratios of the fuels [*Lobert et al.*, 1991; *Hurst et al.*, 1994]. The N/C ratios for different fuel types are readily available from literature [cf. *Crutzen and Andreae*, 1990]. Emissions of CO_2 from biomass burning can be estimated from global inventories of biomass burned for different fuel types [cf. *Hao and Ward*, 1993].

There has been recent interest in acetone as a major source of HO_x radicals in the upper troposphere [*Singh et al.*, 1995]. Our model includes acetone sources of 1.0 Tg C yr⁻¹ from industrial emission, 9 Tg C yr⁻¹ from biomass burning, 12 Tg C yr⁻¹ from the oxidation of propane and higher alkanes, and 15 Tg C yr⁻¹ from vegetation (including both direct emission and secondary production from biogenic hydrocarbons). The vegetation source was adjusted to reproduce aircraft observations of acetone concentrations over the tropical western Pacific and the South Atlantic, as is discussed further by *Wang et al.* [this issue(a)]. Our total acetone source of 37 Tg C yr⁻¹ is at the upper limit of the 25-37 Tg C yr⁻¹ range previously estimated by *Singh et al.* [1994].

Appendix: Chemical Parameterization

Chemical production and loss rates of tracers are computed in the three-dimensional model as parameterized polynomial functions of the ensemble of independent variables defining the chemical environment of the model: tracer concentrations, water vapor, pressure, temperature, solar zenith angle, ozone column, surface albedo, and cloud reflectivities at 800, 500, and 200 mbar. These polynomial functions are used to calculate the following: (1) photolysis rate constants of O_3, NO_2, N_2O_5, HNO_4, HNO_3, PAN, butylnitrate, acetone, methylethyl ketone, and H_2O_2; (2) OH and HO_2 concentrations; (3) partitioning of NO_x as NO, NO_2, NO_3, and HNO_2; (4) chemical production rates of O_3, PANs, butylnitrate, CO, acetone, and methylethyl ketone; and (5) chemical loss rate of O_3. They are constructed by least squares fitting to results from 10,000 photochemical point model calculations spanning the atmospheric ranges of the independent variables [*Spivakovsky et al.*, 1990b]. The point model uses an implicit finite difference kinetic solver and takes randomly selected input values of the independent variables over their respective atmospheric ranges. Radical species and hydrocarbon oxidation intermediates not transported as tracers are assumed to be in chemical steady state in the point model calculations.

The procedure for selecting terms in the polynomial functions is described by *Spivakovsky et al.* [1990b]. The photolysis rate functions include 300 to 400 terms, and the chemical functions include 700 to 900 terms; each term is a product of up to two independent variables with a combined polynomial order of up to 5. Two sets of parameterizations for the photolysis rate functions are constructed for the tropics and the extratropics, and eight sets of parameterizations for the chemical functions are constructed spanning different domains of pressure, temperature, and NO_x concentrations (Table A1) to improve the quality of the least squares fit. Parameterizations including propene and isoprene are constructed only for the atmosphere below 600 mbar because of the short lifetimes of these species.

The quality of a parameterization is evaluated with the root-mean-square relative error (RMSRE):

$$\text{RMSRE} = \exp\left(\sqrt{\frac{1}{n}\sum_{k=1}^{n}\left(\log\left(\frac{y_k}{Y_k}\right)\right)^2}\right) - 1 \qquad (10)$$

where n is the number of an independent set of point model calculations for the parameterization domain ($n = 2000$), Y_k is the output from point model calculation k, and y_k is the corresponding value computed using the parameterization. The RMSREs range from 2 to 4% for the photolysis rate functions; 8 to 19% for OH concentrations; 4 to 25% for HO_2 concentrations; 2 to 15% for NO/NO_x, NO_2/NO_x, and NO_3/NO_x concentration ratios; 9 to 33% for ozone production; 6 to 17% for ozone loss; 20 to 30% for PAN production; 9 to 16% for butylnitrate production; 8 to 40% for CO production; 7 to 17% for acetone production; and 14 to 48% for KET production. RMSREs are smaller for clean than for polluted chemical regimes. Since the RMSREs are computed for randomly chosen points, which include extreme situations not likely to exist in the atmosphere, errors in the three-dimensional model are expected to be smaller. We conducted additional tests of the parameterization functions using multiple-day box model simulations with diurnally varying photolysis rates for polluted

Table A1. Chemical Regimes for the Parameterization Functions

Parameterization Regime	T, K	P, mbar	NO_x, pptv	CO, ppbv	ALK4, pptv	ALKE, pptv	Isoprene, pptv	Acetone, pptv	KET, pptv
A: low altitude, low NO_x, with isoprene	230 - 320	600 - 1,020	0.1 - 400	10 - 400	10 - 20,000	10 - 10,000	10 - 20,000	10 - 10,000	10 - 5,000
B: low altitude, high NO_x, with isoprene	230 - 320	600 - 1,020	400 - 20,000	10 - 400	10 - 20,000	10 - 10,000	10 - 20,000	10 - 10,000	10 - 5,000
C: low altitude, low NO_x, no isoprene	230 - 320	600 - 1,020	0.1 - 400	10 - 400	1 - 20,000	0	0	10 - 10,000	10 - 5,000
D: low altitude, high NO_x, no isoprene	230 - 320	600 - 1,020	400 - 20,000	10 - 400	1 - 20,000	0	0	10 - 10,000	10 - 5,000
E: low altitude, low NO_x, low NMHCs	230 - 320	600 - 1,020	0.1 - 300	10 - 200	1 - 200	0	0	1 - 1,000	1 - 500
F: high altitude, low NO_x	200 - 290	100 - 600	0.1 - 400	10 - 400	1 - 20,000	0	0	10 - 10,000	10 - 5,000
G: high altitude, high NO_x	200 - 290	100 - 600	400 - 20,000	10 - 400	1 - 20,000	0	0	10 - 10,000	10 - 5,000
H: high altitude, low NO_x, low NMHCs	200 - 290	100 - 600	0.1 - 300	10 - 200	1 - 200	0	0	1 - 1,000	1 - 500

The concentration ranges of O_3 (1-250 ppbv), CH_4 (0.5-2 ppmv), ethane (0.01-10 ppbv), and H_2O_2 (0.01-10 ppbv) are the same for all parameterizations; ppmv, parts per million by volume; pptv, parts per trillion by volume. Regimes E and H are subsets of D and G, respectively, and are included to improve the accuracy of the calculation in the remote atmosphere.

and clean conditions and for the upper troposphere; we found good agreement in all cases with results from the implicit finite difference chemical solver (time step of 15 min).

References

Andreae, M. O., E. Atlas, H. Cachier, W. R. Cofer III, G. W. Harris, G. Helas, R. Koppmann, J.-P. Lacaux, and D. W. Ward, Trace gas and aerosol emissions from savanna fires, in *Biomass Burning and Global Change*, vol. 1, *Remote Sensing, Modeling and Inventory Development, and Biomass Burning in Africa*, edited by J. S. Levine, chap. 27, pp. 278-295, MIT Press, Cambridge, Mass., 1996.

Appenzeller, C., J. R. Holton, and K. H. Rosenlof, Seasonal variation of mass transport across the tropopause, *J. Geophys. Res., 101*, 15,071-15,078, 1996.

Atkinson, R. A., D. L. Baulch, R. A. Cox, R. F. Hampson, Jr., J. A. Kerr, and J. Troe, Evaluated kinetic and photochemical data for atmospheric chemistry, supplement IV, IUPAC subcommittee on gas kinetic data evaluation for atmospheric chemistry, *J. Phys. Chem. Ref. Data, 21*, 1125-1568, 1992.

Baldocchi, D. D., B. B. Hicks, and P. Camara, A canopy stomatal resistance model for gaseous deposition to vegetated surfaces, *Atmos. Environ., 21*, 91-101, 1987.

Balkanski, Y. J., and D. J. Jacob, Transport of continental air to the sub-Antarctic Indian Ocean, *Tellus Ser. B, 42*, 62-75, 1990.

Balkanski, Y. J., D. J. Jacob, R. Arimoto, and M. A. Kritz, Long-range transport of radon-222 over the North Pacific Ocean: Implications for continental influence, *J. Atmos. Chem., 14*, 353-374, 1992.

Balkanski, Y. J., D. J. Jacob, G. M. Gardner, W. M. Graustein, and K. K. Turekian, Transport and residence times of continental aerosols inferred from a global three-dimensional simulation of ^{210}Pb, *J. Geophys. Res., 98*, 20,573-20,586, 1993.

Baughcum, S. L., T. G. Tritz, S. C. Henderson, and D. C. Pickett, *Scheduled Civil Aircraft Emission Inventories for 1992: Database Development and Analysis, NASA CR-4700*, Nat. Aeronaut. and Space Admin., Washington, D. C., 1996.

Benkovitz, C. M., T. Scholtz, J. Pacyna, L. Tarrassn, J. Dignon, E. Voldner, P. A. Spiro, J. A. Logan, and T. E. Graedel, Global inventories of anthropogenic emissions of SO_2 and NO_x, *J. Geophys. Res., 101*, 29,239-29,253, 1996.

Bonsang, B., C. Boissard, M. F. Le Cloarec, J. Rudolph, and J. P. Lacaux, Methane, carbon monoxide and light non-methane hydrocarbon emissions from African savanna burnings during the FOS/DECAFE Experiment, *J. Atmos. Chem., 22*, 149-162, 1995.

Box, E., Foliar biomass: Data base of the international biological program and other sources, in *Atmospheric Biogenic Hydrocarbons*, edited by J. Bufalini and R. Arnts, Butterworth-Heinemann, Newton, Mass., 1981.

Bradshaw, J., S. B. Smyth, S. C. Liu, R. Newell, D. D. Davis, and S. T. Sandholm, Observed distributions of nitrogen oxides in the remote free troposphere from NASA Global Tropospheric Experiments, in press, *Rev. Geophys.*, 1998.

Browell, E. V., G. L. Gregory, R. C. Harriss, and V. W. J. H. Kirchhoff, Tropospheric ozone and aerosol distributions across the Amazon Basin, *J. Geophys. Res., 93*, 1431-1451, 1988.

Cahoon, D. R., B. J. Stocks, J. S. Levine, W. R. Cofer, and K. P. O'Neill, Seasonal distribution of African savanna fires, *Nature, 359*, 812-815, 1992.

Cantrell, C. A., et al., Peroxy radicals as measured in ROSE and estimated from photostationary state deviations, *J. Geophys. Res., 98*, 18,355-18,366, 1993.

Chin, M., D. J. Jacob, J. W. Munger, D. D. Parish, and B. G. Doddridge, Relationship of ozone and carbon monoxide over North America, *J. Geophys. Res., 99*, 14,563-14,573, 1994.

Chin, M., D. J. Jacob, G. M. Gardner, M. S. Forman-Fowler, P. A. Spiro, and D. L. Savoie, A global three-dimensional model of tropospheric sulfate, *J. Geophys. Res., 101*, 18,667-18,690, 1996.

Conway, M., and L. L. Liston (Eds.), *The Weather Handbook*, 548 pp., Conway Data, Norcross, Ga., 1990.

Crutzen, P. J., and M. O. Andreae, Biomass burning in the tropics: Impact on atmospheric chemistry and biogeochemical cycles, *Science, 250*, 1669-1678, 1990.

Crutzen, P. J., and P. H. Zimmermann, The changing photochemistry of the troposphere, *Tellus, 43AB*, 136-151, 1991.

DeMore, W. B., S. P. Sander, D. M. Golden, M. J. Molina, R. F. Hampson, M. J. Kurylo, C. J. Howard, and A. R. Ravishankara, Chemical kinetics and photochemical data for use in stratospheric modeling, *JPL Publi. 94-26*, Jet Propul. Lab., Pasadena, Calif., 1994.

Dentener, F. J., and P. J. Crutzen, Reaction of N₂O₅ on tropospheric aerosols: Impact on the global distributions of NOₓ, O₃, and OH, *J. Geophys. Res., 98*, 7149-7163, 1993.

Dignon, J., and J. E. Penner, Biomass burning: A source of nitrogen oxides to the atmosphere, in *Global Biomass Burning: Atmospheric, Climatic and Biospheric Implications*, edited by J. S. Levine, pp. 370-375, MIT Press, Cambridge, Mass., 1991.

Donahue, N. M., M. K. Dubey, R. Mohrschlatdt, K. L. Demerjian, and J. G. Anderson, High-pressure flow study of the reaction NOₓ + OH → HONOₓ: Errors in the falloff region, *J. Geophys. Res., 102*, 6159-6168, 1997.

Drummond, J. W., D. H. Ehhalt, and A. Voltz, Measurement of nitric oxide between 0-12 km altitude and 67°N and 60°S latitude obtained during STRATOZ III, *J. Geophys. Res., 93*, 15,831-15,849, 1988.

EDC-NESDIS, Monthly Global Vegetation Index from Gallo biweekly experimental calibrated GVI (April 1985 - December 1990). Digital raster data on a 10-minute geographic (lat/long) 1080 x 2160 grid, in *Global ecosystems database, version 1.0: Disc A*, edited by NOAA Natl. Geophys. Data Center, Boulder, Colorado, 1992.

Elliott, S., R. P. Turco, and M. Z. Jacobson, Tests on combined projection/forward differencing integration for stiff photochemical family systems at long time step, *Comput. Chem., 17*, 91-102, 1993.

Environmental Protection Agency (EPA), Compilation of air pollution emission factors, *Publ. AP-42*, Washington, D. C., 1985.

Environmental Protection Agency (EPA), The 1985 NAPAP emission inventory (version 2): development of the annual data and modeler's tapes, *Rep. 60017-89-012a*, Research Triangle Park, N. C., 1989.

Environmental Protection Agency (EPA), Supplement F to compilation of air pollutant emission factors, vol. 1, Stationary and point sources, *Rep. AP-42*, Research Triangle Park, N. C., 1993.

Environmental Protection Agency (EPA), National air pollutant emission trends, 1900-1993, *EPA-454/R-94-027*, Research Triangle Park, N. C., 1994.

Erisman, J. W., and A. V. Pul, Parameterization of surface resistance for the quantification of atmospheric deposition of acidifying pollutants and ozone, *Atmos. Environ., 28*, 2595-2607, 1994.

Eugster, W., and R. Hesterberg, Transfer resistances of NO₂ determined from eddy correlation flux measurements over a litter meadow at a rural site on the Swiss plateau, *Atmos. Environ., 30*, 1247-1254, 1996.

Fan, S.-M., S. C. Wofsy, P. S. Bakwin, D. J. Jacob, and D. R. Fitzjarrald, Atmosphere-biosphere exchange of CO₂ and O₃ in the Central Amazon Forest, *J. Geophys. Res., 95*, 16,851-16,864, 1990.

Fehsenfeld, F., J. Calvert, R. Fall, P. Goldan, A. B. Guenther, C. N. Hewitt, B. Lamb, S. Liu, M. Trainer, H. Westberg, and P. Zimmerman, Emissions of volatile organic compounds from vegetation and the implications for atmospheric chemistry, *Global Biogeochem. Cycle, 6*, 389-430, 1992.

Fishman, J., Ozone in the troposphere, in *Ozone in the Free Atmosphere*, edited by R. C. Whitten and S. S. Prasad, pp. 161-194, Van Nostrand Reinhold, New York, 1985.

Fitzjarrald, D. R., K. E. Moore, O. M. R. Cabral, J. Scolar, A. M. Manzi, and L. D. A. Sa, Daytime turbulent exchange between the Amazon Forest and the atmosphere, *J. Geophys. Res., 95*, 16,825-16,838, 1990.

Friedl, R. R. (Ed.), *Atmospheric Effects of Subsonic Aircraft: Interim Assessment Report of the Advanced Subsonic Technology Program, NASA Ref. Publ. 1400*, 168 pp., Nat. Aeronaut. and Space Admin., Greenbelt, Md., 1997.

Gao, W., and M. L. Wesely, Modeling gaseous dry deposition over regional scales with satellite observations, 1, Model development, *Atmos. Environ., 29*, 727-737, 1995.

Goldan, P. D., M. Trainer, W. C. Kuster, D. D. Parish, J. Carpenter, J. M. Roberts, J. E. Yee, and F. C. Fehsenfeld, Measurements of hydrocarbons, oxygenated hydrocarbons, carbon monoxide, and nitrogen oxides in an urban basin in Colorado: Implications for emission inventories, *J. Geophys. Res., 100*, 22,771-22,783, 1995a.

Goldan, P. D., W. C. Kuster, F. C. Fehsenfeld, and S. A. Montzka, Hydrocarbon measurement in the southeastern United States: The Rural Oxidants in the Southern Environment (ROSE) Program 1990, *J. Geophys. Res., 100*, 25,945-25,963, 1995b.

Goldstein, A. H., S. C. Wofsy, and C. M. Spivakovsky, Seasonal variations of nonmethane hydrocarbons in rural New England: Constraints on OH concentrations in northern midlatitudes, *J. Geophys. Res., 100*, 21,023-21,033, 1995.

Guenther, A., et al., A global model of natural volatile organic compound emissions, *J. Geophys. Res., 100*, 8873-8892, 1995.

Hansen, J., G. Russel, D. Rind, P. Stone, A. Lacis, S. Lebedeff, R. Ruedy, and L. Travis, Efficient three-dimensional global models for climate studies: Models I and II, *Mon. Weather Rev., 111*, 609-662, 1983.

Hao, W. M., and D. E. Ward, Methane production from global biomass burning, *J. Geophys. Res., 98*, 20,657-20,661, 1993.

Hao, W. M., M. H. Liu, and P. J. Crutzen, Estimates of annual and regional releases of CO₂ and other trace gases to the atmosphere from fires in the tropics, based on the FAO statistics for the period 1975-1980, in *Proceedings of Third International Symposium on Fire Ecology*, Springer-Verlag, New York, 1990.

Holton, J. R., P. H. Haynes, M. E. McIntyre, A. R. Douglass, R.B. Rood, and L. Pfister, Stratosphere-troposphere exchange, *Rev. Geophys., 33*, 403-439, 1995.

Horowitz, L. W., J. Liang, G. M. Gardner, and D. J. Jacob, Export of reactive nitrogen from North America during summertime, *J. Geophys. Res.*, in press, 1998.

Hurst, D. F., D. W. T. Griffith, J. N. Carras, D. J. Williams, and P. J. Fraser, Measurements of trace gases emitted by Australian savanna fires during 1990 dry season, *J. Atmos. Chem., 18*, 33-56, 1994.

Jacob, D. J., and P. S. Bakwin, Cycling of NOₓ in tropical forest canopies and its implications for the global source of biogenic NOₓ to the atmosphere, in *Microbial Production and Consumption of Greenhouse Gases*, edited by W. B. Whitman, American Society of Microbiology, Washington, D. C., 1991.

Jacob, D. J., and M. J. Prather, Radon-222 as a test of boundary layer convection in a general circulation model, *Tellus Ser. B, 42*, 118-134, 1990.

Jacob, D. J. and S. C. Wofsy, Photochemistry of biogenic emissions over the Amazon forest, *J. Geophys. Res., 93*, 1477-1486, 1988.

Jacob, D. J., and S.C. Wofsy, Budgets of reactive nitrogen, hydrocarbons, and ozone over the Amazon forest during the wet season, *J. Geophys. Res., 95*, 16,737-16,754, 1990.

Jacob, D. J., M. J. Prather, S. C. Wofsy, and M. B. McElroy, Atmospheric distribution of ⁸⁵Kr simulated with a general circulation model, *J. Geophys. Res., 92*, 6614-6626, 1987.

Jacob, D. J., S. Sillman, J. A. Logan, and S. C. Wofsy, Least independent variables method for simulation of tropospheric ozone, *J. Geophys. Res., 94*, 8497-8510, 1989.

Jacob, D. J., et al., Summertime photochemistry of the troposphere at high northern latitudes, *J. Geophys. Res., 97*, 16,421-16,431, 1992.

Jacob, D. J., et al., Simulation of summertime ozone over North America, *J. Geophys. Res., 98*, 14,797-14,816, 1993.

Jacob, D. J., et al., The origin of ozone and NOₓ in the tropical troposphere: A photochemical analysis of aircraft observations over the South Atlantic Basin, *J. Geophys. Res., 101*, 24,235-24,250, 1996.

Kanakidou, M., H. B. Singh, K. M. Valentin, and P. J. Crutzen, A two-dimensional study of ethane and propane oxidation in the troposphere, *J. Geophys. Res., 96*, 15,395-15,413, 1991.

Ko, M. K. W., N. D. Sze, and D. K. Weisenstein, Use of satellite data to constrain the model-calculated atmospheric lifetime for N₂O: Implication for other gases, *J. Geophys. Res., 96*, 7547-7552, 1991.

Koch, D. M., D. J. Jacob, and W. G. Graustein, Vertical transport of tropospheric aerosols as indicated by ⁷Be and ²¹⁰Pb in a chemical tracer model, *J. Geophys. Res., 101*, 18,651-18,666, 1996.

Kramm, G., R. Dlugi, G. J. Dollard, T. Foken, N. Mölders, H. Müller, W. Seiler, and H. Sievering, On the dry deposition of ozone and reactive nitrogen species, *Atmos. Environ., 29,* 3208-3231, 1995.

Laursen, K. K., P. V. Hobbs, L. F. Radke, and R. A. Rasmussen, Some trace gas emissions from North American biomass fires with an assessment of regional and global fluxes from biomass burning, *J. Geophys. Res., 97,* 20,687-20,701, 1992.

Lawrence, M. G., W. L. Chameides, P. S. Kasibhatla, H. Levy II, and W. Moxim, Lightning and atmospheric chemistry: The rate of atmospheric NO production, in *Handbook of Atmospheric Electrodynamics,* vol. 1, edited by H. Volland, chap. 8, pp. 189-202, CRC Press, Boca Raton, Fla., 1995.

Leemans, R., and W. P. Cramer, IIASA mean monthly temperature, precipitation, and cloudiness, in *Global ecosystems database, version 1.0: Disc A,* edited by NOAA Natl. Geophys. Data Center, Boulder, Colorado, 1992.

Levy, H., II, J. D. Mahlman, W. J. Moxim, and S. C. Liu, Tropospheric ozone: The role of transport, *J. Geophys. Res., 90,* 3753-3772, 1985.

Levy, H., II, W. J. Moxim, P. S. Kasibhatla, and J. A. Logan, The global impact of biomass burning on tropospheric reactive nitrogen, in *Global Biomass Burning: Atmospheric, Climatic and Biospheric Implications,* edited by J.S. Levine, pp. 363-369, MIT Press, Cambridge, Mass., 1991.

Levy, H, II., W. J. Moxim, and P. S. Kasibhatla, A global three-dimensional time-dependent lightning source of NO_x, *J. Geophys. Res., 101,* 22,911-22,922, 1996.

Liang, J., and D. J. Jacob, Negligible effect of aqueous-phase cloud chemistry on tropospheric ozone, *J. Geophys. Res., 102,* 5993-6001, 1997.

Liang, J., L. W. Horowitz, D. J. Jacob, Y. Wang, A. M. Fiore, J. A. Logan, G. M. Gardner, and J. W. Munger, Seasonal variation of photochemistry over North America and its implications for the export of ozone and reactive nitrogen to the global atmosphere, *J. Geophys. Res.,* in press, 1998.

Liaw, Y. P., D. L. Sisterson, and N. L. Miller, Comparison of field, laboratory, and theoretical estimates of global nitrogen fixation by lightning, *J. Geophys. Res., 95,* 22,489-22,494, 1990.

Lieth, H., Modeling the primary productivity of the world, in *Primary Productivity of the Biosphere,* edited by H. Lieth and R. Whittaker, Springer-Verlag, New York, 1975.

Lobert, J. M. and D. H. Scharffe, W.-M. Hao, T. A. Kuhlbusch, R. Seuwen, P. Warneck, and P. J. Crutzen, Experimental evaluation of biomass burning emissions: Nitrogen and carbon compounds, in *Global Biomass Burning: Atmospheric, Climatic and Biospheric Implications,* edited by J. S. Levine, MIT Press, Cambridge, Mass., 1991.

Logan, J. A., Nitrogen oxides in the troposphere: Global and regional budgets, *J. Geophys. Res., 88,* 10,785-10,807, 1983.

Logan, J. A., M. J. Prather, S. C. Wofsy, and M. B. McElroy, Tropospheric chemistry: A global perspective, *J. Geophys. Res., 86,* 7210-7254, 1981.

Lurmann, F. W., A. C. Lloyd, and R. Atkinson, A chemical mechanism for use in long-range transport/acid deposition computer modeling, *J. Geophys. Res., 91,* 10,905-10,936, 1986.

Mano, S., Messung von partiell oxidierten Kohlenwasserstoffen in Emissionen von Biomasseverbrennung, Ph.D. thesis, 120 pp., Goethe-Universitat, Frankfurt, Germany, 1995.

Martinere, P., G. P. Brasseur, and C. Granier, The chemical composition of ancient atmosphere: A model study constrained by ice core data, *J. Geophys. Res., 100,* 14,291-14,304, 1995.

Matthews, E., Global vegetation and land use: New high resolution data bases for climate studies, *J. Chem. Appl. Meteorol., 22,* 474-487, 1983.

McElroy, M. B., R. J. Salawitch, and K. Minschwaner, The changing stratosphere, *Planet. Space Sci., 40,* 373-401, 1992.

McKeen, S. A., T. Gierczak, J. B. Burkholder, P. O. Wennberg, T. F. Hanisco, E. R. Keim, A. R.-S. Gao, S. C. Liu, A. R. Ravishankara, and D. W. Fahey, The photochemistry of acetone in the upper troposphere: A source of odd-hydrogen radicals, *Geophys. Res. Lett., 24,* 3177-3180, 1997.

Menaut, J. C., L. Abbadie, F. Lavenu, P. Loudjani, and A. Podaire, Biomass burning in west African savannas, in *Global Biomass Burning: Atmospheric, Climatic and Biospheric Implications,* edited by J. S. Levine, pp. 133-142, MIT Press, Cambridge, Mass., 1991.

Metwally, M., *Jet Aircraft Engine Emissions Database Development-- 1992 Military, Charter, and Nonscheduled Traffic, NASA CR-4684,* Nat. Aeronaut. and Space Admin., Washington, D. C., 1995.

Michelsen, H. A., R. J. Salawitch, P. O. Wennberg, and J. G. Anderson, Production of O^1D from photolysis of O_3, *Geophys. Res. Lett., 21,* 2227-2230, 1994.

Middleton, P., W. R. Stockwell, and W. P. L. Carter, Aggregation and analysis of volatile organic compound emissions for regional modeling, *Atmos. Environ., 24A,* 1107-1133, 1990.

Müller, J.-F., and G. Brasseur, IMAGES: A three-dimensional chemical transport model of the global troposphere, *J. Geophys. Res., 100,* 16,445-16,490, 1995.

Munger, J. W., S. C. Wofsy, P. S. Bakwin, S.-M. Fan, M. L. Goulden, B. C., Daube, A. H. Goldstein, K. E. Moore, and D. R. Fitzjarrald, Atmospheric deposition of reactive nitrogen oxides and ozone in a temperate deciduous forest and a subarctic woodland, 1, Measurements and mechanisms, *J. Geophys. Res., 101,* 12,639-12,657, 1996.

Murphy, D. M., D. W. Fahey, M. H. Proffitt, S. C. Liu, K. R. Chan, C. S. Eubank, S. R. Kawa, and K. K. Kelly, Reactive nitrogen and its correlation with ozone in the lower stratosphere and upper troposphere, *J. Geophys. Res., 98,* 8751-8773, 1993.

Nance, J. D., P. V. Hobbs, and L. R. Radke, Airborne measurements of gases and particles from an Alaskan wildfire, *J. Geophys. Res., 98,* 14,873-14,882, 1993.

Norman, J., Simulation of microclimates, in *Biometeorology in Integrated Pest Management,* Academic, San Diego, Calif., 1982.

Norton, F., Regulation of tropical climate by radiation, ocean circulation, and atmospheric dynamics, Ph.D. thesis, 102 pp., Harvard Univ., Cambridge, Mass., 1996.

Olson, J., World ecosystems (WE1.4): Digital raster data on a 10 minute geographic 1080 x 2160 grid, in *Global ecosystems database, version 1.0: Disc A,* edited by NOAA Natl. Geophys. Data Center, Boulder, Colorado, 1992.

Olson, J., et al., Results from the Intergovernmental Panel on Climate Change photochemical model intercomparison (PHOTOCOMP), *J. Geophys. Res., 102,* 5979-5991, 1997.

Paulson, S. E., and J. H. Seinfeld, Development and evaluation of a photooxidation mechanism for isoprene, *J. Geophys. Res., 97,* 20,703-20,715, 1992.

Penner, J. E., S. S. Atherton, J. Dignon, S. J. Ghan, and J. J. Walton, Tropospheric nitrogen: A three-dimensional study of sources, distributions, and deposition, *J. Geophys. Res., 96,* 959-990, 1991.

Piccot, S. D., J. J. Watson, and J. W. Jones, A global inventory of volatile organic compound emissions from anthropogenic sources, *J. Geophys. Res., 97,* 9897-9912, 1992.

Prather, M. J., M. B. McElroy, S. C. Wofsy, G. Russell, and D. Rind, Chemistry of the global troposphere: Fluorocarbons as tracers of air motion, *J. Geophys. Res., 92,* 6579-6613, 1987.

Press, W. H., S. A. Teukolskey, W. T. Vetterling, and B. P. Flannery, *Numerical Recipes in FORTRAN: The Art of Scientific Computing,* 2nd ed., Cambridge Univ. Press, New York, 1992.

Price, C., and D. Rind, A simple lightning parameterization for calculating global lightning distributions, *J. Geophys. Res., 97,* 9919-9933, 1992.

Price, C., and D. Rind, Modeling global lightning distributions in a general circulation model, *Mon. Weather Rev., 122,* 1930-1939, 1994.

Price, C., J. Penner, and M. Prather, NO_x from lightning, 1, Global distribution based on lightning physics, *J. Geophys. Res., 102,* 5929-5941, 1997a.

Price, C., J. Penner, and M. Prather, NO_x from lightning, 2, Constraints from the global atmospheric electric circuit, *J. Geophys. Res., 102,* 5943-5951, 1997b.

Roelofs, G.-J., and J. Lelieveld, Distribution and budget of O_3 in the troposphere calculated with a chemistry general circulation model, *J. Geophys. Res., 100,* 20,983-20,998, 1995.

Rudolph, J., The tropospheric distribution and budget of ethane, *J. Geophys. Res., 100,* 11,369-11,381, 1995.

Rutledge, S. A., E. R. Williams, and T. D. Keenan, The down under Doppler and electricity experiment (DUNEE): Overview and preliminary results, *Bull. Am. Meteorol. Soc., 73,* 3-16, 1992.

Samaras, Z., and K.-H. Zierock, Summary report of the CORINAIR working group on emission factors for calculating 1985 emissions from road traffic, vol. 3, 38 pp., Commission of Europ. Communities, Luxembourg, 1989.

Seinfeld, J. H., *Atmospheric Chemistry and Physics of Air Pollution*, 594 pp., John Wiley, New York, 1986.

Shaw, R. H., Wind movement within canopies, in *Biometeorology in Integrated Pest Management*, Academic, San Diego, Calif., 1982.

Singh, H. B., D. O'Hara, D. Herlth, W. Sachse, D. R. Blake, J. D. Bradshaw, M. Kanakidou, and P. J. Crutzen, Acetone in the atmosphere: Distribution, sources, and sinks, *J. Geophys. Res.*, *99*, 1805-1819, 1994.

Singh, H. B., M. Kanakidou, P. J. Crutzen, and D. J. Jacob, High concentrations and photochemical fate of oxygenated hydrocarbons in the global troposphere, *Nature*, *378*, 50-54, 1995.

Smyth, S.B., et al., Factors influencing the upper free tropospheric distribution of reactive nitrogen over the South Atlantic during the TRACE-A Experiment, *J. Geophys. Res.*, *101*, 24,165-24,186, 1996.

Spivakovsky, C. M., and Y. J. Balkanski, Tropospheric OH: Constraints imposed by observations of ¹⁴CO and CH₃CCl₃, in *Report of the WMO-sponsored Meeting of Carbon Monoxide (CO) Experts*, edited by P. C. Novelli and R. M. Rosson, Global Atmos. Watch, World Meteorol. Organ., Geneva, 1994.

Spivakovsky, C. M., R. Yevich, J. A. Logan, S. C. Wofsy, M. B. McElroy, and M. J. Prather, Tropospheric OH in a three-dimensional chemical trace model: An assessment based on observations of CH₃CCl₃, *J. Geophys. Res.*, *95*, 18,441-18,472, 1990a.

Spivakovsky, C. M., S. C. Wofsy, and M. J. Prather, A numerical method for parameterization of atmospheric chemistry: Computation of tropospheric OH, *J. Geophys. Res.*, *95*, 18,433-18,440, 1990b.

Stordal, F., R. G. Derwent, I. S. A. Isaksen, D. J. Jacob, M. Kanakidou, J. A. Logan, and M.J. Prather, Model simulation of global tropospheric ozone, in *Scientific Assessment of Ozone Depletion: 1994, Rep. 37*, Global Ozone Res. and Monit. Proj., World Meteorol. Organ., Geneva, 1995.

Tang, I. N., and H. R. Munkelwitz, Water activities, densities, and refractive indices of aqueous sulfate and nitrate droplets of atmospheric importance, *J. Geophys. Res.*, *99*, 18,801-18,808, 1994.

Thompson, A. M., M. A. Huntley, and R. W. Stewart, Perturbations to tropospheric oxidants, 1985-2035, 1, Calculation of ozone and OH

in chemically coherent regions, *J. Geophys. Res.*, *95*, 9829-9844, 1990.

Trenberth, K. E., Global analyses from ECMWF and atlas of 1000 to 10 mb circulation statistics, *NCAR/TN-373+STR*, Natl. Center for Atmos. Res., Boulder, Colo., 1992.

Wang, Y., J. A. Logan, and D. J. Jacob, Global simulation of tropospheric O₃-NOₓ-hydrocarbon chemistry, 2, Model evaluation and global ozone budget, this issue(a).

Wang, Y., D. J. Jacob, and J. A. Logan, Global simulation of tropospheric O₃-NOₓ-hydrocarbon chemistry, 3, Origin of tropospheric ozone and effects of nonmethane hydrocarbons, this issue(b).

Warneck, P., *Chemistry of the Natural Atmosphere*, 753 pp., Academic, San Diego, Calif., 1988.

Wesely, M. L., Parameterization of surface resistance to gaseous dry deposition in regional-scale numerical models, *Atmos. Environ.*, *23*, 1293-1304, 1989.

Wesely, M. L., and B. B. Hicks, Some factors that affect the deposition rates of sulfur dioxide and similar gases on vegetation, *J. Air Pollut. Control Assoc.*, *27*, 1110-1116, 1977.

Williams, E. R., Large-scale charge separation in thunderclouds, *J. Geophys. Res.*, *90*, 6013-6025, 1985.

World Meteorological Organization (WMO), *Scientific Assessment of Ozone Depletion: 1994, Rep. 37*, Global Ozone Res. and Monit. Proj., World Meteorol. Organ., Geneva, 1995.

Yienger J. J. and H. Levy II, Empirical model of global soil-biogenic NOₓ emissions, *J. Geophys. Res.*, *100*, 11,447-11,464, 1995.

D. J. Jacob and J. A. Logan, Department of Earth and Planetary Sciences and Division of Engineering and Applied Sciences, Harvard University, Cambridge, MA 02138. (e-mail: djj@io.harvard.edu; jal@io.harvard.edu)

Y. Wang, School of Earth and Atmospheric Sciences, Georgia Institute of Technology, Atlanta, GA 30332-0340. (e-mail: yhw@eas.gatech.edu)